Real-time, wide field-of-view monitoring of the atmosphere by means of a novel imaging lidar system

Kohei Shinomiya[1], Kenji Masuda[1], Masanori Yabuki[1], Makoto Sasaki[2], Hiroaki Kuze[1]

[1] *Center for Environmental Remote Sensing, Chiba University, 1-33 Yayoi-cho, Inage-ku, Chiba 263-8522, Japan, hkuze@faculty.chiba-u.jp, shinomiya@graduate.chiba-u.jp*

[2] *Institute for Cosmic Ray Research, University of Tokyo, 5-1-5 Kashiwa-no-Ha, Kashiwa City Chiba 277-8582, Japan, sasakim@icrr.u-tokyo.ac.jp*

Abstract

An imaging lidar system has been constructed on the basis of the All-sky Survey High Resolution Air-shower (Ashra) telescope, originally developed for detecting cosmic-ray particles with extremely high energy. In this study, we describe the system performance of the imaging lidar system, including the noise-reduction capabilities and its application to aerosol and cloud monitoring.

Keywords: aerosol, imaging lidar

1. Introduction

The remarkable features of the All-sky Survey High Resolution Air-shower (Ashra) telescope system are a wide field-of-view (FOV) (40×40 deg), high angular resolution (1 arcmin = 0.29 mrad), and a high-speed, highly sensitive imaging system with an intelligent triggering capability.[1)] By employing this novel telescope, we have constructed an imaging lidar system[2)] for monitoring aerosols and clouds in the troposphere. In the bistatic mode of operation, the telescope is placed apart from the laser source. While the laser beam direction is scanned in the FOV range of the telescope, the scattered light is detected in the scattering-angel range of $0<\theta<180$ deg. Although bistatic measurements of aerosols have so far been reported[3,4)] the laser beam direction was mostly fixed near the zenith direction, giving the detection near the backscattering scheme. In contrast, forward scattering yields high signal-to-noise ratio (S/N) owing to the general property of the Mie scattering from aerosols. Since the wavelength range of the Ashra telescope is in the UV range of 300-420 nm, here the bistatic measurement is made using the laser wavelength of 351 nm. This ensures relatively eye-safe lidar operation, since the level of maximum permissible exposure (MPE) is very high in the UV compared with the visible wavelength region.

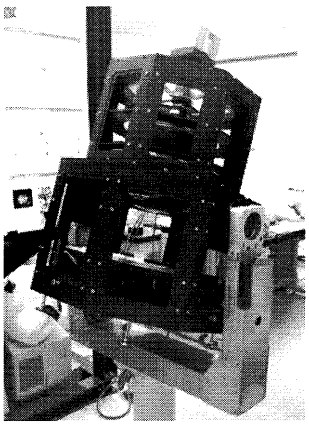

Fig. 1 1/3-scale Ashra telescope image

2. 1/3-Scale Ashra telescope

The 1/3-scale Ashra telescope (Fig. 1) is equipped with a 60-cm diameter main mirror and three corrector lenses (Baker-Nunn system), as shown in the schematic (Fig. 2). A UV-pass absorption filter is used to eliminate the longer wavelength light. The image is formed at the input plane of a 6-inch electro-static image intensifier (II, Toshiba TETD), which reduces the size of the image to about 13 mm. The resulting image, in turn, is sent through a high-speed gated II (Hamamatsu) and detected by a cooled CCD camera (Bitran, BN51LN). The field-of-view angle and the angular resolution of this telescope system have been measured to be 31 deg and 4.3 arcmin (1.26 mrad), respectively.

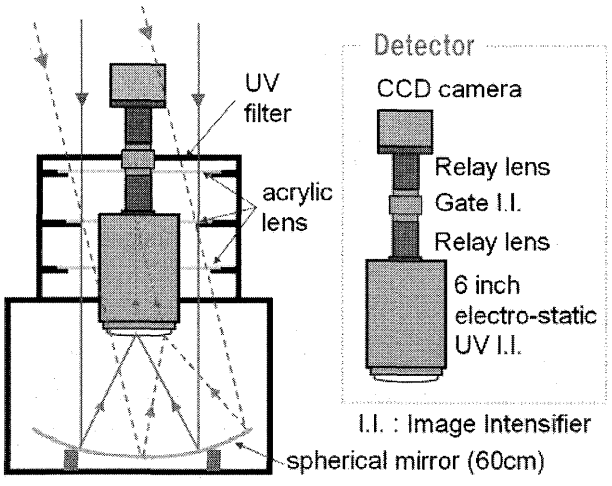

Fig. 2 Schematic of 1/3-scale Ashra telescope

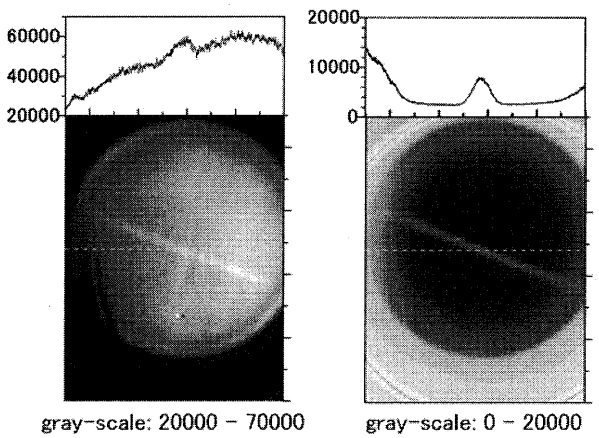

Fig. 3 Images obtained from the imaging lidar observation: (a) continuous mode, and (b) gated mode with a gate width of 20 μs,: exposure time 1s, repetition rate 800Hz

The elimination of background light is important in the imaging lidar measurement. We have applied the gating synchronized with the laser pulse repetition rate (800 Hz). As shown in Fig. 3, the background noise due to the night skylight is reduced to a level of a few percent.

3. Bistatic lidar theory

In the bistatic measurement, a laser and a telescope are located separately, with a baseline distance of L (Fig. 4). The laser is illuminating a direction θ_{laser} in elevation, while the telescope is observing the beam path toward a direction θ_{view}. In this bistatic measurement, the lidar equation is written as

$$P = P_0 \; K \; \frac{A}{r^2} \; ds \; \beta(\theta_{scat}) \; T, \qquad (1)$$

where P is the received signal intensity, P_0 the emitted laser intensity, K the efficiency of the receiving optics, A the area of the telescope mirror, r the distance between the target (aerosol particle) and the telescope, θ_{scat} the scattering angle, and T the transmittance along the combined laser path and viewing path. The portion of the laser beam path subtended by the FOV for a single pixel of the array detector is denoted as ds, which is given as

$$ds = \frac{r \; \theta_{FOV}}{\sin(\theta_{scat})} \; . \qquad (2)$$

The side-scattering coefficient, $\beta(\theta_{scat})$, is defined as

$$\beta(\theta_{scat}) = \alpha_1 \; f_1(\theta_{scat}) + \alpha_2 \; f_2(\theta_{scat}) \; . \qquad (3)$$

Here, θ_{FOV} is the FOV for a single pixel, α the extinction coefficient, and f the phase function. Subscript 1 is for aerosol and 2 for air molecule. Combining Eqs.(1) and (2), one can see that the signal is proportional to r^{-1}, indicating less stringent requirement for the system dynamic range.

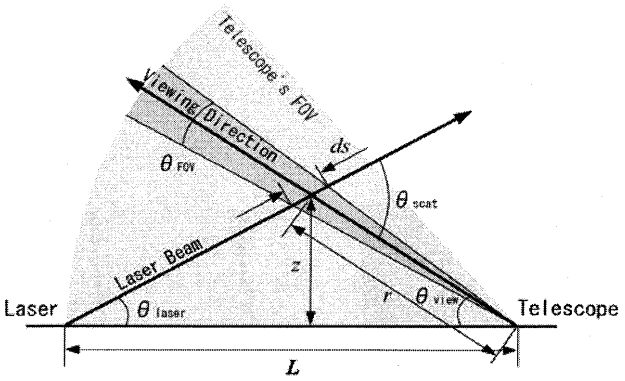

Fig. 4 Configuration of bistatic lidar measurement

4. Bistatic observation

The bistatic observation was carried out by locating the Ashra telescope at about 40 m from the laser location. The experimental setup is shown in Fig. 5. The telescope axis was fixed toward the zenith, so that when the elevation angle of the 351 nm laser beam was 60 deg, for instance, laser traces are recorded in an altitude range of 50-130 m. The exposure time was 1 s and the gate width was 20 μs.

Fig. 6(a) shows the laser traces obtained by subtracting the background (laser-off) image from the laser-on image. Fig. 6(b) shows the resulting intensity obtained by accumulating the digital number (DN) values across the laser beam trace. Comparison between the experimental result (Fig. 6(b)) and

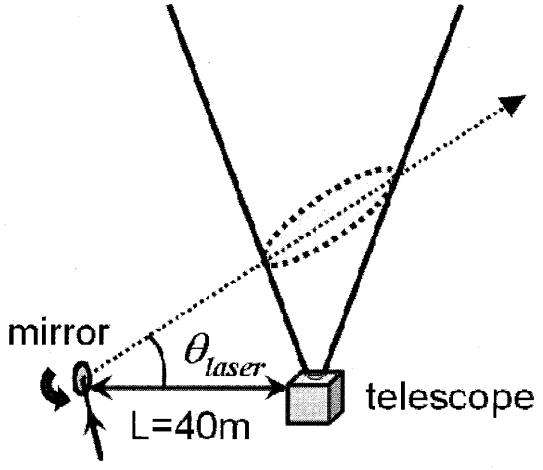

Fig. 5 Experimental setup for the bistatic measurement with the Ashra telescope

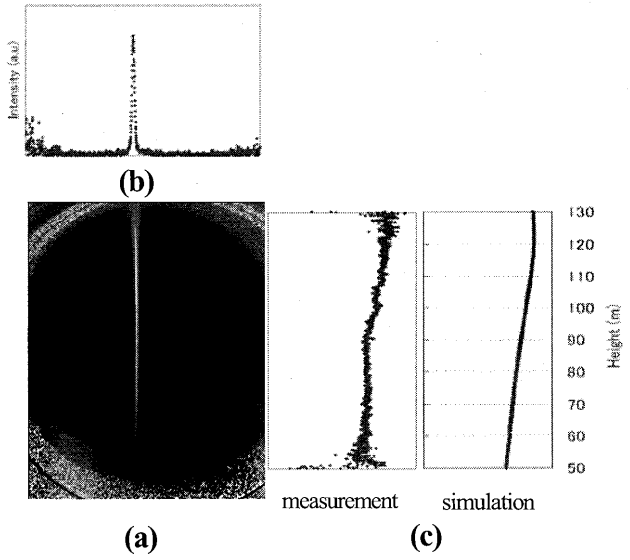

Fig. 6 (a) image of the UV laser beam, (b) cross- sectional signal intensity and (c) measured and simulated intensity of the scattered light.

simulation (Fig. 6(c)) indicates that we have a reasonable agreement between them. Because of the high-sensitivity of the Ashra telescope, it is possible to obtain two-dimensional distributions of aerosols and clouds by scanning the laser beam direction in the telescope FOV.

5. Cloud observation using the Ashra telescope

Fig. 7 shows an example of cloud images continuously observed with the Ashra telescope system. In this experiment, both the laser beam and telescope axis directions were fixed vertically. The bright spot indicates the point at which the laser beam hits the cloud bottom, where multiple scattering effects occasionally causes the spatial spread of return images.

For the sake of quantitative evaluation of cloud optical properties, we have undertaken a simulation in which the imaging lidar observation using the Ashra telescope can be exploited to derive the information on cloud droplet sizes. The following form of C1 cloud distribution is assumed:

$$n(r) = C\left(\frac{r}{R_m}\right)^{\nu_p} \exp\left(-\frac{r \cdot \nu_p}{R_m}\right) \qquad (4)$$

Here C is a normalization constant and r is the particle radius. The parameter ν_p stands for the width of the distribution, and R_m is the geometrically averaged mean radius: here we fix ν_p=6, while varying R_m in a range of 1-20 μm (1 μm step) (Fig. 8). The Mie theory for spherical particles is employed to calculate the scattering phase function assuming the complex refractive of m= 1.33-0.00i. Fig. 9 shows the resulting phase functions for various values of the droplet mean radius, R_m. In this figure, the variation is shown in the scattering angle (θ_{scat}) range of 170-180 deg, with all the curves normalized at θ_{scat} =180 deg. As seen from this figure, maxima in phase functions appear in the rage of θ_{scat} = 174 -179 deg. This result indicates that a close examination of this scattering angle regime might enable determination of droplet radius for clouds having R_m<10 μm.

Next, we consider the case in which the elevation angle of the laser beam is fixed and only the position of laser emission is changed (Fig. 10). In this case we assume an elevation angle of 85 deg. Fig. 11 shows the relation

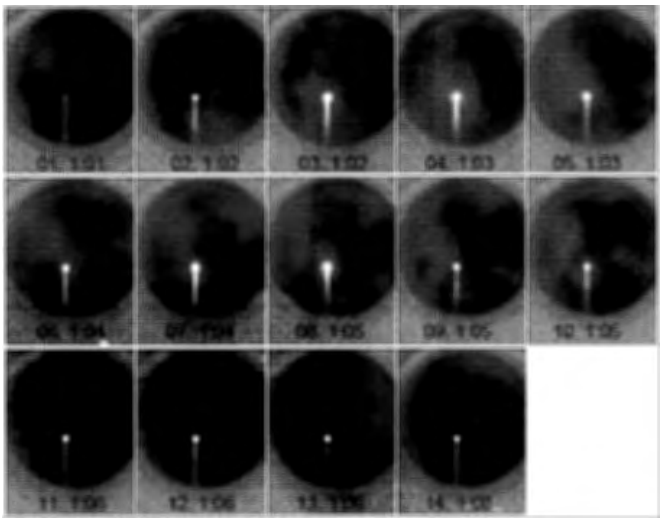

Fig. 7 Temporal change of cloud return with the vertically emitted laser beam.

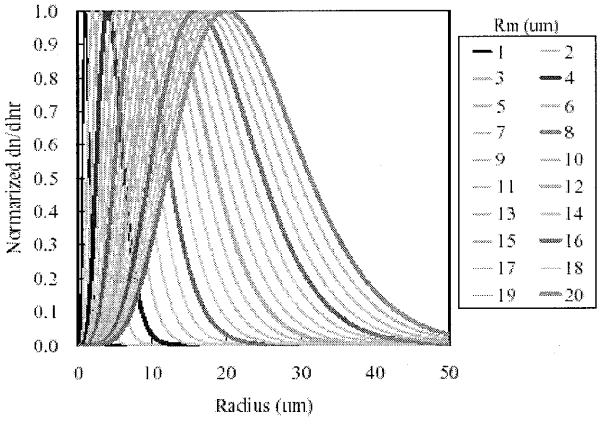

Fig. 8 Size distribution of cloud droplets assumed in the present simulation

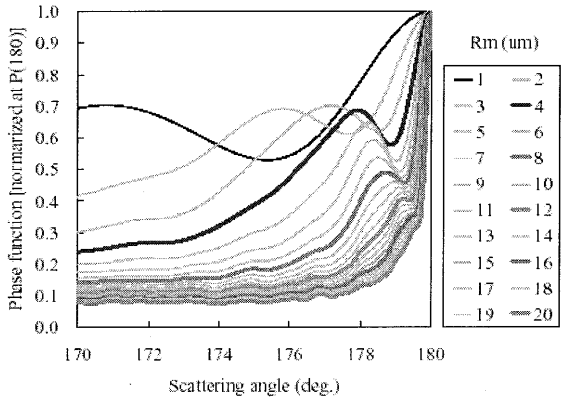

Fig. 9 Variation of phase function for various values of droplet mean radius

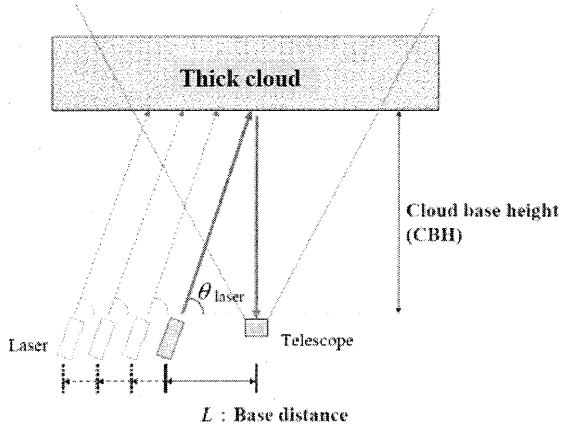

Fig. 10 Proposed observation scheme

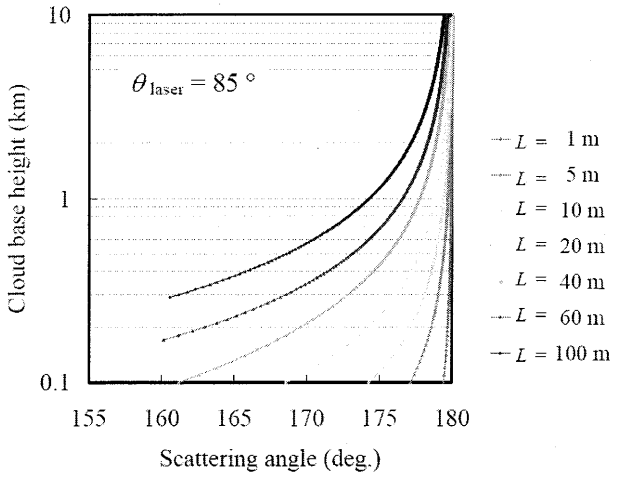

Fig. 11 Relation between the cloud base height and the observational range of the scattering angle for various distances between the laser and telescope

between the cloud base height and the observational range of the scattering angle for various distances between the laser and telescope. When the base distance L is changed between 1 and 100 m, the possible range of the scattering angle is 161.2 - 179.4 deg the cloud base height (CBH) of 100 m, 168.6 - 179.9 deg for CBH = 500 m, and 177.7 - 179.9 for CBH = 1 km. Since the present measurement of the Ashra telescope can be carried out with L = 5 to 40 m, one can see that observations with θ_{scat} =175.6 - 179.4 deg is feasible for clouds with CBH = 500 m, and θ_{scat} =177.8 - 179.7 deg for those with CBH = 1 km, leading to coverage of the scattering angle range which characterizes the variation in the phase functions as shown in Fig. 9.

Details on the relevant experiment will be shown in the presentation.

Acknowledgements

This work was supported by the Grant-in-aid for Scientific Research from the Ministry of Education, Culture, Sports, Science and Technology, Japan.

References

1) Sasaki, M. A. Kusaka, Y. Asaoka, 2002: Design of UHECR telescope with 1 arcmin resolution and 50°field of view, Nucl. Instr. Meth. Phys. Res. A492, 49-56.

2) Kouga, I. Y. Yamaguchi, S. Fukagawa, N. Takeuchi, H. Kuze, M. Sasaki, Y. Asaoka, S.Ogawa, 2006: Bistatic Measurement of Atmospheric Aerosol Distributions by Using an Imaging Lidar, Proc.23rd Int. Laser Radar Conf., 211-214.

3) Meki, K., K. Yamaguchi, X. Li, Y. Saito, T.D. Kawahara, and A. Nomura, 1996: Range-resolved bistatic imaging lidar for the measurement of the lower atmosphere, Opt. Lett. 21 (17), 1318-1320.

4) Barnes, J.E., S. Bronner, R. Beck, N. C. Parikh, 2003: Boundary Layer Scattering Measurements with a Charge-Coupled Device Camera Lidar, Applied Optics, 42 (15), 2647-2652.